Influence of Probe Local Flow Field Distortion on Measurement Results of Ultrasonic Flowmeter

W. L. Chen[1,2] , C. H. Li[3], and J. Mu[2]

[1] College of Civil Engineering and Mechanics, Lanzhou University, Lanzhou, China;
[2] Xinjiang Institute of Measurement & Testing Technology, No. 188, hebei east road, xinshi district, Urumqi, China
[3] National Institute of Metrology, Beijing, China
E-mail: chenwl16@lzu.edu.cn

Abstract

The installation of the intrusive probe will disturb the internal flow field inside the ultrasonic flowmeter, which will affect the measurement results. Probe protruded into the flow or recessed into the wall is one of the most important uncertainty sources of ultrasonic transit-time flowmeters. There are three ways to install the probe of the ultrasonic flowmeter in the pipeline: fully convex installation (the probe protrudes into the pipeline), fully concave installation (the probe is installed to form a depression on the pipe wall) and tangent installation (the center line of the probe is flush with the pipe wall, a part of the probe protrudes from the pipe, and a depression is also formed on the pipe wall).

In this paper, for the small and medium-diameter ultrasonic flowmeters with double-sided 8-channel arrangement, numerical simulations are carried out under the fully convex, fully concave and tangent probe installation modes, respectively. By analyzing the flow field distribution near the probe and the change of the velocity profile on the path line, the physical mechanism of the influence of the flow separation caused by the mainstream flow near the probe on the measurement results of the ultrasonic flowmeter is revealed. Then the influence of probe disturbance on the measurement results of ultrasonic flowmeter under different pressure and flow rate was analyzed by experiments, and the error correction model is proposed according to the experimental results. The research contents provide a theoretical basis for the installation and use of ultrasonic flowmeter.

1. Introduction

The installation mode of the intrusive probe inside the pipeline will affect the measurement results of the ultrasonic flowmeter, which includes two aspects[1]. One is that the path length changes due to the intrusion of the probe into the pipe wall, which leads to measurement errors. Such errors can be eliminated by measuring the path length. Second, the probe will produce local disturbance in the flow field[2].

It is mentioned in IEC41 that the protrusion or depression of the probe on the inner wall of the pipeline will affect the measurement of the ultrasonic flowmeter. When the probe is protruding, the length of the path is reduced, thereby reducing the volume flow of the pipe, resulting in negative errors; when the probe is concave, grooves will be formed on the inner wall of the pipe, resulting in distortion of the flow field. The low negative error depends on the design and installation of the ultrasonic sensor. The sensor must be verified by CFD analysis or hydraulic laboratory testing when the ratio of protrusion to path length exceeds 0.25%.

In IEC41, a certain analysis has been made for large pipe diameters, but the condition of sound path length below 1 m is not mentioned. and the influence of the local disturbance caused by the recessed and tangent probe installation methods on the measurement results of the ultrasonic flowmeter has not been analyzed. Existing related research results are mainly aimed at large-diameter ultrasonic flowmeters[3, 4]. For medium and small-diameters, the influence of transducers on measurement is more serious. In general, there are relatively few researches on the flow measurement error introduced by the insertion type ultrasonic flowmeter probe[5]. The researchers' understanding of the probe disturbance is still insufficient. Some manufacturers are not clear about which installation method can introduce the smallest measurement error due to lack of experience[6].

In this paper, by analyzing the flow field distribution near the probe and the change of the velocity profile on the path line[7], the physical mechanism of the influence of the flow separation caused by the mainstream flow near the probe on the measurement results of the ultrasonic flowmeter is revealed. Then the influence of probe disturbance on the measurement results of ultrasonic flowmeter under different pressure and flow rate was analyzed by experiments, and the error correction model is proposed according to the experimental results.

2. Numerical simulation modeling and meshing of probe local turbulence

2.1 Build the model

According to different ultrasonic flowmeter probe installation methods, simplified models of ultrasonic flowmeters with different probe installation methods are built in ICEM. The insertion depth of the probe under different installation methods is shown in Figure 1. There are three types: full convex (Figure 1a), tangent (Figure 1b) and full concave (Figure 1c). The length of the path length increases with the change of the installation method, as shown in Figure 1d. The diameter *D* of the pipeline is 100mm, and the length of the middle ultrasonic flow meter body section is 3*D*. There is a 10*D* straight pipe upstream of the ultrasonic flowmeter and a 5*D* straight pipe downstream to ensure that the fluid in the pipeline can form a fully developed flow. The diameter of the probe is 12 mm, and the angle between the path line and the pipe axis is 60° .

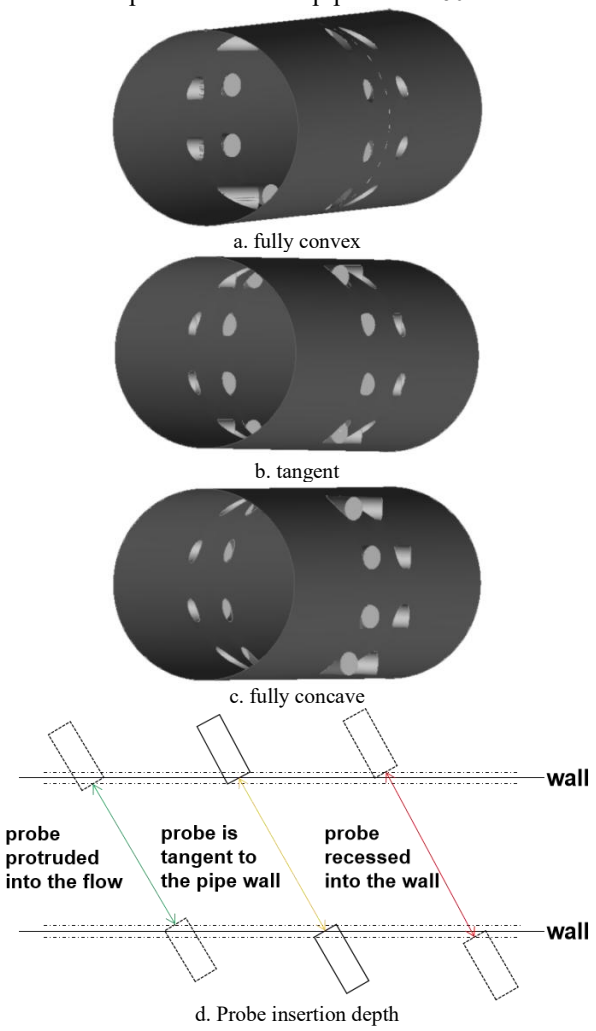

Figure 1: Simplified models of different probe installation methods.

The path position is arranged according to the Gauss-Jacobi integration scheme as shown in Table 1. The average surface velocity is the weighted sum of the velocities along the individual paths. For a single measurement section, the flow is calculated according to formula 1. And for a two-section measurement, the final flow rate was the average of the measured volumetric flow rates of the two sections.

$$Q = R\sum_{i=1}^{n} w_i v_i L_{wi} \sin\varphi \qquad (1)$$

Table 1: Integral parameters of ultrasonic flowmeter corresponding to Gauss-Jacobi method

Path No.	path height ratio d_i	Weight factor w_i
1	0.8090	0.3693
2	0.3090	0.5976
3	-0.3090	0.5976
4	-0.8090	0.3693

The path lengths under different probe installation methods are shown in Table 2.

Table 2 Path length under different installation methods

Installation method	Path No.	Path length（mm）
protrusion	1（4）	42.5
	2（3）	100.7
tangent	1（4）	67.9
	2（3）	109.8
recess	1（4）	86.4
	2（3）	117.9

2.2 Meshing and calculation parameter settings

The model adopts tetrahedral unstructured mesh, and the boundary layer is densified, as shown in Figure 2. After verifying the independence of the meshes, it was determined that the overall mesh count was approximately 1.5 million. This can not only ensure that the grids near the probe are dense enough, but also control the overall number of grids and improve the efficiency of simulation calculation.

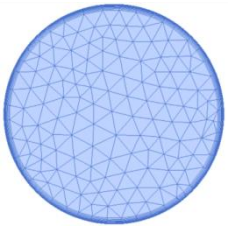

Figure 2: Wall boundary layer meshing

After mesh division is completed, mesh files are imported into Fluent for calculation.

The inlet condition is set as the velocity inlet. In the simulation process, it is generally considered that the flow at the inlet of the flow field is a fully developed flow, and the velocity direction at the inlet of the flow field is perpendicular to the inlet section and parallel to the axis of the pipeline.

The outlet condition is set as outflow, and the position was set at 5D downstream of the flowmeter. The boundary outside the inlet and outlet is set as the solid wall boundary under the adiabatic no-slip condition.

The parallel channel arrangement and channel numbers are shown in Figure 3. They are paths 1/2/3/4 respectively from top to bottom.

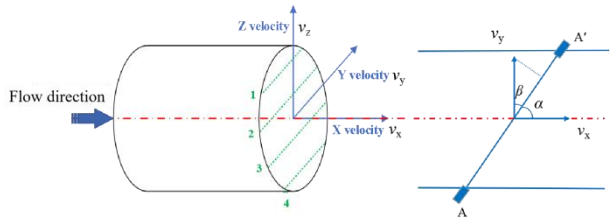

Figure 3: The angle between parallel channel arrangement and each axial direction.

3. Analysis of numerical simulation results

3.1 Verification of Simulation Results

In order to verify the reliability of the CFD simulation results, the simulation and real-flow results under the tangent probe installation mode were compared, so as to ensure that the calculation results of the simulation simulation and the real-flow experiments can confirm each other. Table 3 shows the comparison between the simulation data and the experimental results when the tangent probe is installed in a straight pipe and the inlet velocity v is 4 m/s and 15 m/s respectively.

Table 3: Comparison between simulation results and experimental results

Results	Velocity m/s	Calculated flow rate m^3/h	Reference flow m^3/h	E %
Simulation	4	97.82	103.04	-5.07
Experiment		105.566	107.33	-1.64
Simulation	15	367.17	394.29	-6.88
Experiment		393.153	402.12	-2.23

3.2 Comparison of flow field distribution of different probe installation methods

In the fully convex and tangent probe installation mode, the probe protrudes completely or partially from the pipe wall and extends into the pipe interior, forming a wedge block with OMNP node, as shown in Figure 4. When the viscous fluid flows to point O, it is forced to rise along the wedge-shaped flow surface to form a climbing flow. In the process of the viscous fluid flowing from point O to point M, the velocity increases and the pressure decreases, that is to say $\frac{dp}{dx} < 0$.

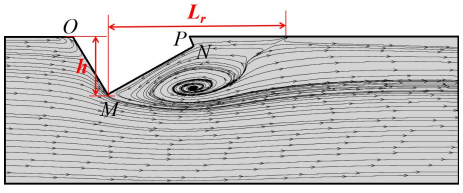

a. The fully convex type

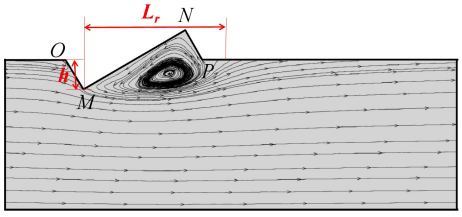

b. The tangent type

Figure 4: The probe extends into the internal flow field of the pipeline to form the diagram of reflux area.

The force caused by the pressure gradient will push the fluid particles forward, forming a flow process of depressurization and acceleration; in this part of the flow process, only the viscous blocking effect of the surface is opposite to the direction of the fluid motion, but the viscous blocking effect can only Slowing down the fluid flow rate, it is impossible to cause the fluid to move in the opposite direction, so no boundary layer separation occurs. Assuming that the climbing flow velocity is V, the climbing flow velocity can be decomposed after passing through the vertex M of the wedge block to form axial velocity $V\cos\alpha$ and normal velocity $V\sin\alpha$, as shown in Figure 5.

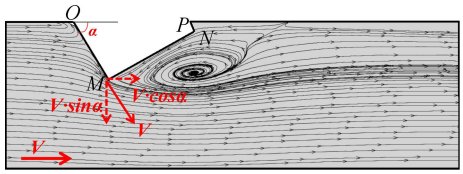

Figure 5: Velocity decomposition of climbing flow

And when the climbing flow flows through the wedge-shaped vertex M, the potential flow achieves the maximum velocity at the point M, here $\frac{dp}{dx} = 0$. After the point M, there is $\frac{dp}{dx} > 0$, and with the increase of x, the degree of $\frac{dp}{dx} > 0$ increased gradually. During the process of the fluid flows to the point N, due to the combined influence of the reverse pressure gradient and the viscous stagnation effect of the object surface, the fluid near the object surface is continuously decelerated, and finally stagnates because the inertial force cannot overcome the above resistance. The flow in the boundary layer separates from the surface of the probe and generates vortexes behind it, that is, backflow appears at the back end of the upstream probe.

Because the flow resistance in the boundary layer consumes energy, the pressure at point N is lower than that at point O. Therefore, cavitation will be formed in the downstream of the probe after boundary layer separation, which is also the reason for dirt accumulation in the downstream of the probe.

Figure 6 shows the velocity distribution with the probe installation mode of fully convex.

As can be seen from Figure 6a, under the installation mode of fully-convex probe, the throttling effect of upstream probe is obvious, and strong backflow occurs near the probe. Besides, the distance between upstream probe of A1 path and downstream probe of B1 path is close, resulting in the influence of upstream probe of A1 path on the fluid will spread to the measurement area near downstream probe of B1 path. The upstream probes of path B1 have the same effect on the downstream probes of path A1.

For path A2 and B2, see Figure 6b, the distance between the downstream probe and the upstream probe of symmetric path is relatively far, and the influence of the upstream probe of symmetric path is small. At the same time, the path length is shortened in the fully convex probe installation mode, and the upstream and downstream return areas are larger, resulting in the shortest intermediate flow area.

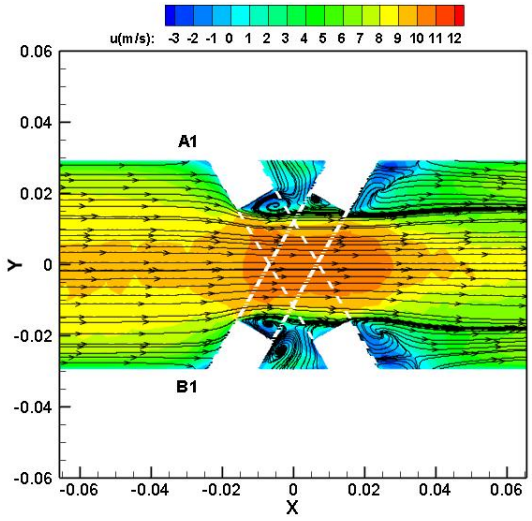

a. Streamline diagram of the plane where the path 1 is located.

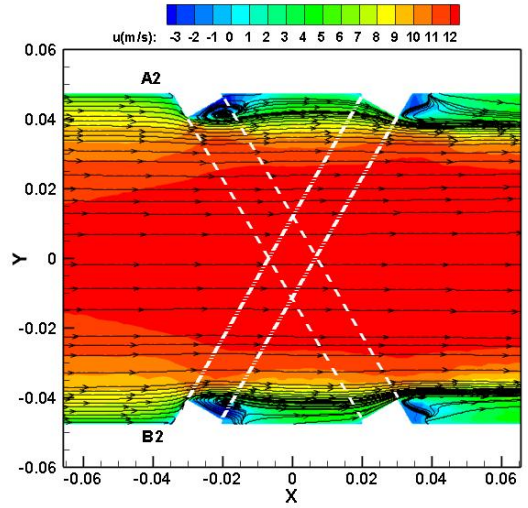

b. Streamline diagram of the plane where the path 2 is located.

Figure 6: Velocity distribution with the fully convex probe installation mode.

Figure 7 shows the velocity distribution with the installation mode of tangent probes.

In the tangent probe installation mode, due to the small height h of the wedge block, the length L_r of the upstream return area on the path 1/4 and the path 2/3 is smaller than that in the fully-convex installation mode, and the downstream probe is not affected, and the difference between path 1/4 and path 2/3 is not significant.

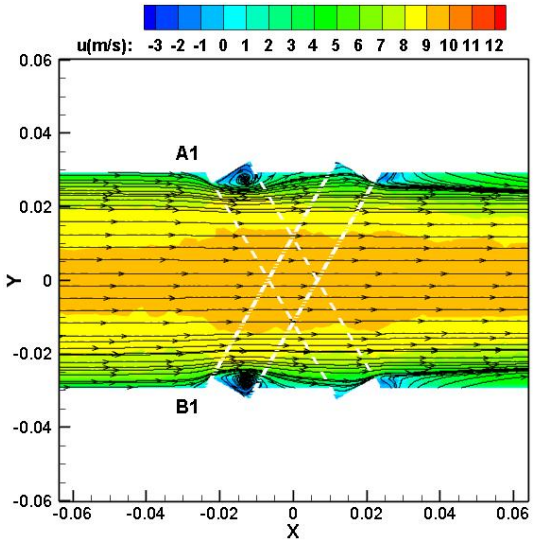

a. Streamline diagram of the plane where the path 1 is located.

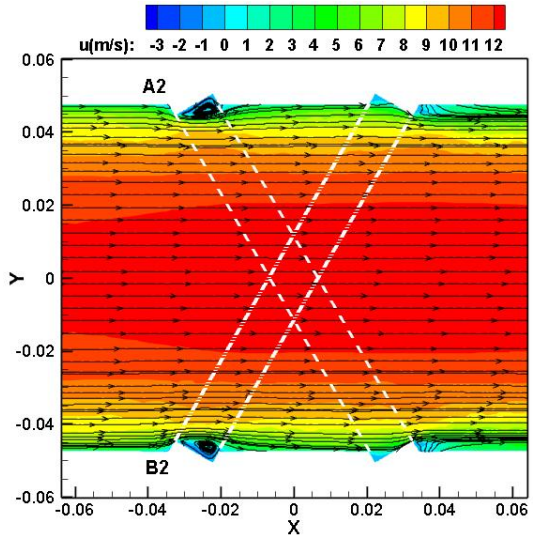

b. Streamline diagram of the plane where the path 2 is located.

Figure 7: Velocity distribution with the tangent probe installation mode.

In the fully concave probe installation mode, when the fluid passes through the depressions of the upstream and downstream probes, it will flow back in the grooves, forming negative pressure, and vortices will be generated in the grooves, resulting in negative velocity at both ends of the path line, which will eventually lead to negative error.

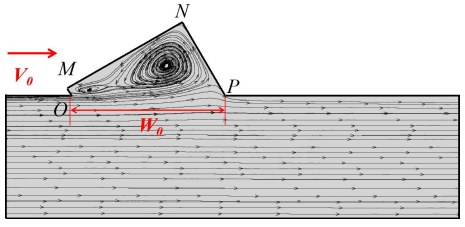

Figure 8: Schematic diagram of the probe recessed in the tube wall to form a recirculation zone.

It can be seen from Figure 9a that when the fluid passes through the upstream groove, small vortices will be formed at the bottom of corners. The small vortices

cover a small area of the channel line, while in the downstream groove, there is a large vortex covering the entire groove width. The width of the vortex layer in the downstream groove is larger than that in the upstream groove, so it can be considered that the cyclic volume of independent vortices in the downstream groove is larger than that in the upstream groove. Since the width of the upstream and downstream grooves is the same, it can be inferred that the negative velocity of the downstream groove is greater than that of the upstream groove, which will be significantly reflected on the velocity profile.

Compared with path 1/4, path 2/3 have shallower grooves and fewer vortices in the upstream grooves, and larger vortices cover the channel lines, resulting in relatively obvious negative velocities both upstream and downstream, see Figure 9b.

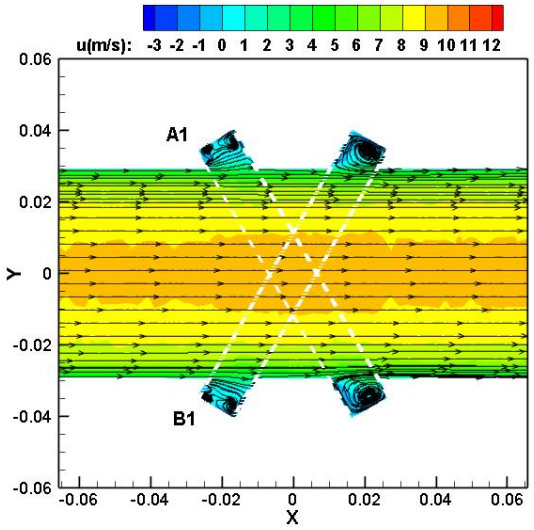

a. Streamline diagram of the plane where the path 1 is located.

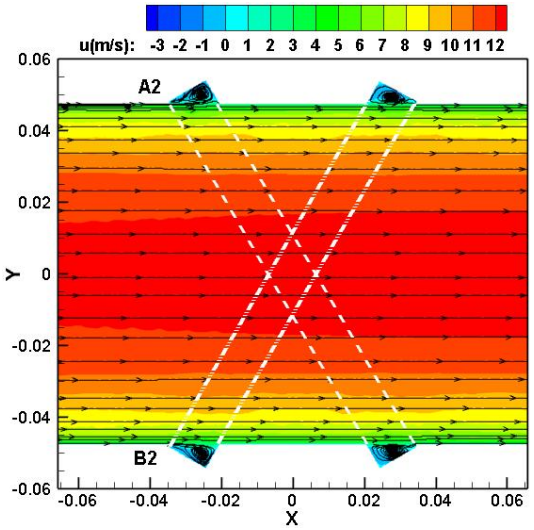

b. Streamline diagram of the plane where the path 2 is located.

Figure 9: Velocity distribution with the fully concave probe installation mode.

Figure 10 shows the velocity profiles of different probe installation methods. Compared with the upstream 2D reference position, in the fully convex probe installation mode, the length L_i of each path is shortened because the probe protrudes into the pipe. Therefore, the velocity distribution of each path in the measurement section is narrower than that at the upstream 2D. There is a backflow at the upstream probe, so that there is a negative velocity at the upstream end of the path line. At the same time, it is precisely because of the throttling effect of the deep installation of the probe that the flow area of the fluid when it flows near the probe becomes smaller, resulting in an increase in the flow velocity in the middle area of the pipeline, which is reflected in the fact that the flow velocity value in the middle part of the channel in the measurement section is higher than that at the upstream 2D.

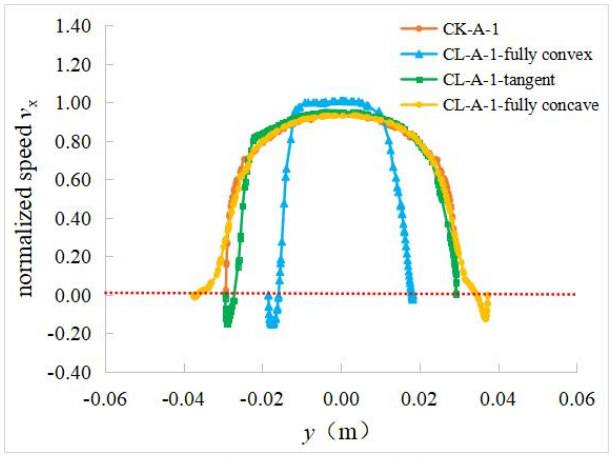

a. Velocity profile on path 1/4

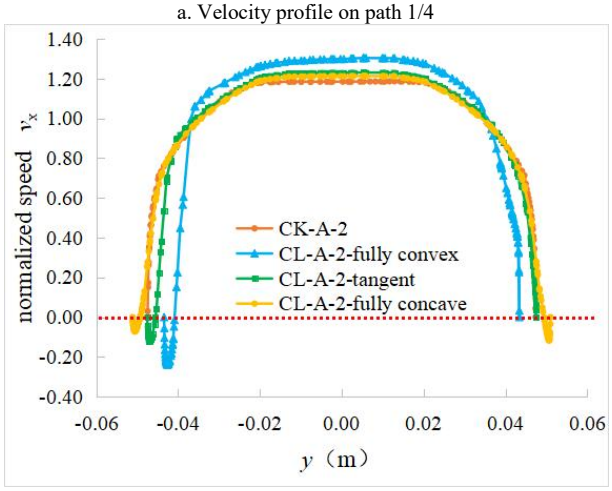

b. Velocity profile on path 2/3

Figure 10: Velocity profiles of different probe installation methods.

In the tangent probe installation mode, the path length at the measurement section is the same as that in the reference state, but because the probe is half deep into the pipeline, there is a negative velocity near the upstream probe, that is, the speed near the upstream position is lower than that in the reference state, but the speed near the centerline of the path is also slightly increased compared to the reference state due to the throttling effect.

In the fully concave probe installation mode, the probe forms a depression on the pipe wall, the path length at the measurement section is longer than that in the reference state. At the same time, due to the existence of the depression, there is a backflow near the

upstream and downstream probes. For path 1 and 4, the negative velocity in the downstream groove is greater than the negative velocity in the upstream groove, which makes the velocity curve asymmetric; for path 2 and 3, the negative velocity formed in the upstream and downstream grooves is asymmetric.

3.3 Comparison of relative errors of simulation results of different probe installation methods

Figure 11 visually shows the change of the indication error of the ultrasonic flowmeter measurement section under different probe installation methods, where the abscissa is the logarithmic coordinate of the Reynolds number. It can be seen from the Figure 10 that the simulation results under different probe installation methods are quite different, and under the same probe installation method, with the increase of the flow rate (or Reynolds number), the error is also different. The specific analysis is as follows:

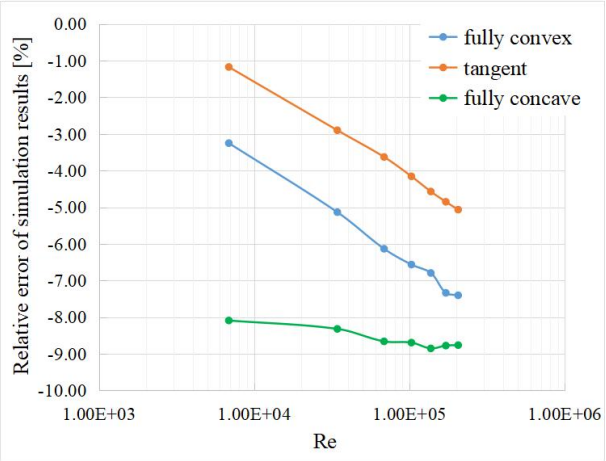

Figure 11: Comparison of measurement results under different probe installation methods.

- The measurement error E_{sim} of ultrasonic flowmeter is negative no matter which probe installation mode.
- Under the same probe installation method, the measurement error increases with the increase of velocity value or Reynolds number, and tends to be stable after increasing to a certain value.
- The relative error is tangent < fully convex < fully concave, the tangent double-sided eight-channel probe installation method has the best installation effect, the maximum error is -5.067%, the convex installation method is next, the maximum error is -7.404%, the concave probe installation method has the worst effect, the maximum error reached -8.853%.
- In the fully convex and tangent probe installations, there is a linear relationship between the indication error and the logarithm of Reynolds number. However, when the fully-concave probe is installed, the indication error changes little with the Reynolds number and the linearity of the measurement result is good. In this case, a single correction coefficient K can be used to correct the measurement result Q to obtain a good result, that is $Q' = K \cdot Q$, the specific correction coefficient K depends on the probe shape, size, installation angle, etc.

4. Experimental results and error correction model of ultrasonic flowmeter under the installation of tangent probe

The physical mechanism of the influence of probe local turbulence on the measurement results of ultrasonic flowmeter is understood by numerical simulation. The simulation results show that the effect of the tangent probe installation on the ultrasonic flowmeter is relatively small, and the measurement error is more consistent with the Reynolds number. In this section, the ultrasonic flowmeter with tangent probe installation is calibrated by real flow experiment, and a modified model is proposed according to the experimental results.

During the experiment, the DN100 mm ultrasonic flowmeter on the high-pressure loop air flow standard device of China NIM was selected for the experiment under the pipeline pressures of 0.36 MPa, 1.3 MPa and 2.5 MPa, respectively. Figure 12 shows the experimental results of the DN100mm ultrasonic flowmeter under different pressures on the high-pressure air flow standard device.

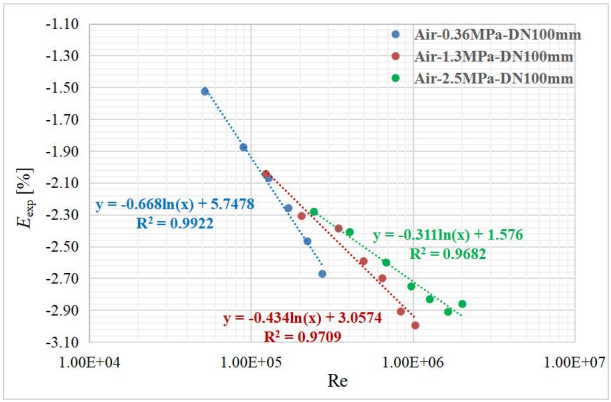

Figure 12: Experimental results of DN100mm ultrasonic flowmeter on high pressure air flow standard device

The error of the experimental results is smaller than that of the simulation results, but its change trend is consistent with the error change trend of the tangent probe installation method in the simulation results.

Under the same pressure, the indication error decreases gradually with the increase of Reynolds number, and there is a linear relationship between the indication error and the logarithm of the Reynolds number, as shown in Formula 2. The coefficients a and b are different under different pressures. The measurement results of the DN100mm ultrasonic flowmeter can be corrected by Formula 2. The corrected errors are shown in Table 4.

$$E_{exp} = a \times \ln \mathrm{Re} + b \qquad (2)$$

Table 4: Corrected error of DN100mm ultrasonic flowmeter on high pressure air device

0.36 MPa		1.3 MPa		2.5 MPa	
Re	Corrected	Re	Corrected	Re	Corrected

	error (%)		error (%)		error (%)
51841.28	-0.023	123454.10	-0.015	244645.00	0.001
89769.63	-0.006	205344.07	-0.057	407818.45	0.032
129001.64	0.043	347487.06	0.093	684785.28	0.002
170144.37	0.039	496353.77	0.042	977368.19	-0.038
223113.27	0.011	648524.17	0.051	1272608.32	-0.036
275804.64	-0.052	843242.62	-0.044	1650673.37	-0.035
		1035711.61	-0.042	2022996.31	0.078

5. Conclusion

In this paper, for the small and medium-diameter ultrasonic flowmeter with double-sided 8-path arrangement based on the Gauss-Jacobi integration method, numerical simulations are carried out under the fully convex, tangent and fully concave probe installation modes, respectively. The angle of the profile line and the length of the effective channel line was analyzed. The physical mechanism of the influence of the local turbulence of the probe on the measurement results of the ultrasonic flowmeter was analyzed, and the reason for the difference between the errors introduced by different probe installation methods was analyzed.

The real-flow experiment calibration is carried out for the ultrasonic flowmeter with the tangent probe installation method. The results show that the errors caused by the local turbulence of the probe to the ultrasonic flowmeter are all negative values. The error of DN100mm ultrasonic flowmeter is concentrated in (-3.1%~-1.5%). Under the same pressure, the indication error gradually decreases with the increase of Reynolds number, and the difference between indication error and the logarithm of Reynolds number shows Linear relationship, and the error correction model was proposed.

References

[1]. Drenthen J. G., de Boer G. The manufacturing of ultrasonic gas flow meters[J]. Flow Measurement and Instrumentation, 2001, 12 (2): 89-99.

[2]. Voser A., Staubli T. CFD calculations of the protrusion effect and impact on the acoustic discharge measurement accuracy. In 1st International Conference on Hydraulic Efficiency Measurements, Montreal, 1996.

[3]. Zheng D. D., Zhang P. Y., Xu T. S. Study of acoustic transducer protrusion and recess effects on ultrasonic flowmeter measurement by numerical simulation[J]. Flow Measurement & Instrumentation, 2011, 22 (5): 488-493.

[4]. Wang B., Cui Y., Liu W., et al. Study of Transducer Installation Effects on Ultrasonic Flow Metering Using Computational Fluid Dynamics[J]. Advanced Materials Research, 2013, 629: 676-681.

[5]. Renaldas R. Investigation of the flow velocity profile in a metering section of an invasive ultrasonic flowmeter[J]. Flow Measurement & Instrumentation, 2006, 17 (4): 201-206.

[6]. Roman V., Matiko F., Kostyk I. Investigation of Turbulence Parameters Influence on Results of CFD Modeling of Flow in Ultrasonic Flowmeter[J]. Energy engineering and control systems, 2021, 7 (1): 73-78.

[7]. Arnould P. An investigation into the performance and diagnostics from different chordal integration schemes in asymmetric flow[J]. Flow Measurement and Instrumentation, 2020, 72 101144.